

This is the accepted manuscript made available via CHORUS. The article has been published as:

## First g-factor measurements of the $2_{1}^{+}$ and the $4_{1}^{+}$ states of radioactive $^{100}\text{Pd}$

D. A. Torres, G. J. Kumbartzki, Y. Y. Sharon, L. Zamick, B. Manning, N. Benczer-Koller, G. Gürdal, K.-H. Speidel, M. Hjorth-Jensen, P. Maier-Komor, S. J. Q. Robinson, T. Ahn, V. Anagnostatou, M. Elvers, P. Goddard, A. Heinz, G. Ilie, D. Radeck, D. Savran, and V. Werner

Phys. Rev. C **84**, 044327 — Published 25 October 2011

DOI: [10.1103/PhysRevC.84.044327](https://doi.org/10.1103/PhysRevC.84.044327)

# First $g$ -factor measurements of the $2_1^+$ and the $4_1^+$ states of radioactive $^{100}\text{Pd}$

D.A. Torres,\* G.J. Kumbartzki, Y.Y. Sharon, L. Zamick, B. Manning, and N. Benczer-Koller

*Department of Physics and Astronomy, Rutgers University, New Brunswick, NJ 08903, USA*

G. Gürdal

*Nuclear Engineering Division, Argonne National Laboratory, Argonne, Illinois 60439, USA*

K.-H. Speidel

*Helmholtz-Institut für Strahlen- und Kernphysik, Universität Bonn, Nussallee 14-16, D-53115 Bonn, Germany*

M. Hjorth-Jensen

*Department of Physics and Center of Mathematics for Applications, University of Oslo, N-0316 Oslo, Norway*

P. Maier-Komor

*Physik-Department, Technische Universität München, James-Frank-Str., D-85748 Garching, Germany*

S.J.Q. Robinson

*Department of Physics, Millsaps College, Jackson, Mississippi 39210, USA*

T. Ahn, V. Anagnostatou,<sup>†</sup> M. Elvers,<sup>‡</sup> P. Goddard,<sup>†</sup> A. Heinz,<sup>§</sup> G. Ilie, D. Radeck,<sup>‡</sup> D. Savran,<sup>¶</sup> and V. Werner

*Wright Nuclear Structure Laboratory, Yale University, New Haven, Connecticut 06520, USA*

The  $g$  factors of the first  $2^+$  and  $4^+$  states of the radioactive  $^{100}\text{Pd}$  nucleus have been investigated for the first time, using an alpha-particle transfer reaction from  $^{12}\text{C}$  to  $^{96}\text{Ru}$ . The transient magnetic field technique in inverse kinematics was used. The  $^{100}_{46}\text{Pd}_{54}$  nucleus is a suitable candidate for studying single-particle proton and neutron effects in the nuclear wave functions near the  $N = Z = 50$  shell closures. The results are discussed within the frameworks of both large-scale shell-model calculations and collective-model predictions.

PACS numbers: 21.10.Ky, 25.70.Hi, 27.60.+j

---

\* datorresg@physics.rutgers.edu

<sup>†</sup> Also at: Department of Physics, University of Surrey, Guildford, GU2 5XH, United Kingdom

<sup>‡</sup> Also at: Institut für Kernphysik, Universität zu Köln, Zùlpicher Str.77, D-50937 Köln, Germany

<sup>§</sup> Present address: Department of Fundamental Physics, Chalmers University of Technology, SE-412 96 Gothenburg, Sweden

<sup>¶</sup> Also at: Institut für Kernphysik, Technische Universität Darmstadt, Schlossgartenstr.9, D-64289 Darmstadt, Germany; Present address: ExtreMe Matter Institute EMMI and Research Division, GSI Helmholtzzentrum für Schwerionenforschung GmbH, Planckstr. 1, D-64291 Darmstadt, Germany

## I. INTRODUCTION

The transitional even- $A$  Pd nuclei (with  $Z = 46$ ), in the  $A \sim 100$  region close to the  $Z = N = 50$  shell closures, present excellent opportunities to study the interplay between single-particle and collective degrees of freedom, and have been recently investigated both experimentally and theoretically [1–4]. For the specific case of the radioactive  $^{100}_{46}\text{Pd}_{54}$  nucleus ( $T_{1/2} = 3.63$  d), excited states have been explored using  $\gamma$ -ray spectroscopy. In a recent work by Radeck et al., the authors used the fusion-evaporation reaction  $^{99}\text{Ru}(^3\text{He}, 2n)^{100}\text{Pd}$  to populate and study states in  $^{100}\text{Pd}$  [4]. The  $2_1^+$ ,  $4_1^+$ ,  $6_1^+$  sequence of yrast states, at almost equally spaced energies, strongly suggests the signature of an almost pure vibrational behavior. The corresponding experimental  $B(E2)$  values, larger than 20 W.u., show a collective enhancement that is consistent with the vibrational picture. Sambataro and Dieperink [5] carried out a theoretical study of the  $g$  factors of the  $2_1^+$  states for nuclei in this region, using the collective Interacting Boson Approximation-2 (IBA-2). They obtained for  $^{100}\text{Pd}$  a value of  $g(2_1^+) = +0.4$ , close to the prediction of the simple collective model of  $g_{\text{collective}} = Z/A = 0.46$ . On the other hand, large-scale shell-model calculations for  $^{100}\text{Pd}$  yield good agreement with the experimental excitation energies and  $B(E2)$  transition strengths [4, 6]. The proximity of this nucleus to the  $Z = N = 50$  shell closures suggests that a single-particle picture may indeed be relevant. Until now, no experimental information on  $g$  factors was available for  $^{100}\text{Pd}$ .

Since neither an intense beam nor a target of the radioactive  $^{100}\text{Pd}$  isotope is currently available, it is not possible to perform experiments on this nucleus using Coulomb excitation reactions in inverse or conventional kinematics. However,  $^{100}\text{Pd}$  nuclei can be produced by the transfer of one  $\alpha$  particle from a carbon target to the beam ions of  $^{96}\text{Ru}$  nuclei. This reaction favors the population of low-spin states, with some spin alignment and with appreciable recoil velocities which permit the application of the transient field technique in inverse kinematic conditions. The Bonn group has previously used  $\alpha$ -transfer reactions to study  $g$  factors in radioactive isotopes in the  $A \sim 40$  [7, 8] and  $A \sim 60$  [9, 10] regions.

In the present work, the  $\alpha$ -transfer technique has been extended to the  $A \sim 100$  region. The current paper reports on the  $g$ -factor measurements of the  $2_1^+$  and  $4_1^+$  states in the radioactive  $^{100}\text{Pd}$  nucleus. Simultaneously, the  $g$  factors of the  $2_1^+$  and the  $4_1^+$  states of  $^{96}\text{Ru}$  were measured by Coulomb excitation of the beam. These latter results will be discussed in a forthcoming paper [11].

## II. EXPERIMENTAL PROCEDURE AND DATA ANALYSIS

The interaction of the nuclear magnetic moment of a given nuclear state with the transient magnetic field results in a spin precession proportional to the  $g$  factor of this state [12]. The experimental setup is schematically shown in Fig. 1.

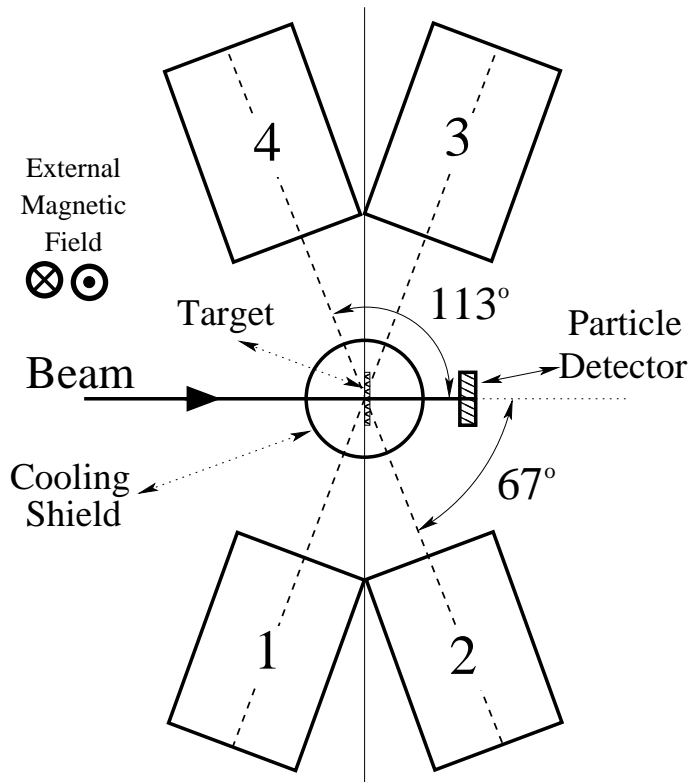


FIG. 1. The setup used in the experiment. Clover detectors 2 and 3 were placed at  $\pm 67^\circ$  with respect to the beam, while clovers 1 and 4 were placed at  $\pm 113^\circ$ . The particle detector was positioned behind the target.

### 1. Reaction

Excited states in  $^{100}\text{Pd}$  were populated using the reaction  $^{12}\text{C}(^{96}\text{Ru}, ^8\text{Be})^{100}\text{Pd}$ . An isotopically pure beam of  $^{96}\text{Ru}$ , with intensities of  $\sim 1$  pA, was accelerated to an energy of 350 MeV at the ESTU Tandem accelerator of the Wright Nuclear Structure Laboratory at Yale University. The experiment utilized a multilayered target consisting of  $0.61$  mg/cm<sup>2</sup> of carbon, deposited on  $6.42$  mg/cm<sup>2</sup> of gadolinium, which in turn was evaporated on a  $1.0$  mg/cm<sup>2</sup> thick tantalum foil, backed by  $5.6$  mg/cm<sup>2</sup> of copper. The evaporation of the gadolinium layer on the tantalum foil provides the best magnetic properties for the target [13]. The  $^{12}\text{C}$  layer provides the environment for both  $\alpha$ -transfer

and Coulomb-excitation reactions, producing highly forward-focused  $^{12}\text{C}$  ions and  $\alpha$  particles from the decay of  $^8\text{Be}$ , with distinct energies for each reaction. The  $\alpha$ -transfer reaction occurs at beam energies just above the Coulomb barrier ( $\sim 335$  MeV), with one  $\alpha$  particle being transferred from a  $^{12}\text{C}$  nucleus to a  $^{96}\text{Ru}$  nucleus, forming  $^{100}\text{Pd}$ . The residual  $^8\text{Be}$  nucleus is unstable and decays within  $10^{-16}$  s into two  $\alpha$  particles [9, 14] which are detected by a particle detector located in the forward direction, behind the target (see Fig. 1). Due to the inverse kinematics of the reaction, the  $^{100}\text{Pd}$  nuclei travel forward through the gadolinium layer of the target at high velocities ( $\langle v \rangle \sim 0.05$  c). The nuclear spins of the  $^{100}\text{Pd}$  excited states precess in the transient magnetic field (TF) of the gadolinium layer [12]. The transit time of the  $^{100}\text{Pd}$  ions through the gadolinium layer is about 0.6 ps. The  $^{100}\text{Pd}$  nuclei are subsequently stopped in the hyperfine-interaction-free copper backing. The  $^{96}\text{Ru}$  beam itself was stopped by an additional 11.2 mg/cm<sup>2</sup> copper foil placed downstream from the target.

## 2. External magnetic field

The orientation of the TF is controlled by the direction of the magnetic field in the gadolinium layer. The magnetization was maintained by an external magnetic field,  $B_{ext} = 0.07$  T, applied alternately in the up ( $\uparrow$ ) and down ( $\downarrow$ ) directions with respect to the  $\gamma$ -ray detection plane. The external magnetic field direction was changed every 136 sec. The magnetization  $M$  of the target was measured, offline, as a function of the temperature, before the experiment, in an AC magnetometer [15]. It was found to be  $M = 0.1795$  tesla, and approximately constant between 50 K and 120 K. During the experiment, the conditions were chosen to minimize the heating of the target above 120 K, where the magnetization of the gadolinium is reduced. There is, as of now, no reliable method to measure the actual temperature of the beam spot. Hence, the target frame was kept at 60 K by a closed-cycle Displex Cryocooler; a low beam current was utilized ( $< 1$  pA) with a large and defocussed beam profile (a 4 mm diameter collimator was used). A cylindrical copper cooling shield, with an opening for the beam and an exit for the light particles, was placed around the target [1].

## 3. Gamma-ray and particle detection

The gamma rays corresponding to the de-excitation of the states of the  $^{100}\text{Pd}$  nucleus were detected in four Canberra clover HP-Ge detectors, placed at symmetrical angles around the center of the target (see Fig. 1). Each clover is composed of four non-segmented HPGe crystals (Eurogam Clover type in Ref. [16]). The clover detectors were

all located at distances of about 130 mm from the target. Clover detectors 2 and 3 were placed at  $\pm 67^\circ$  with respect to the beam, while clovers 1 and 4 were placed at  $\pm 113^\circ$ . The scattered light particles were detected in a circular ( $300 \text{ mm}^2$ ) PIPS Canberra Silicon detector subtending an angle of  $\pm 26^\circ$ . Particle and  $\gamma$ -ray energies were recorded, with their respective time stamps, as single events, using a PIXIE-4 digital pulse-processing multichannel data-acquisition system from XIA [17]. Particle- $\gamma$  ray and  $\gamma$ - $\gamma$  coincidence matrices were constructed off-line using the time difference information between events. The analysis employed the spectrum analysis codes XSA [18] and Tv [19].

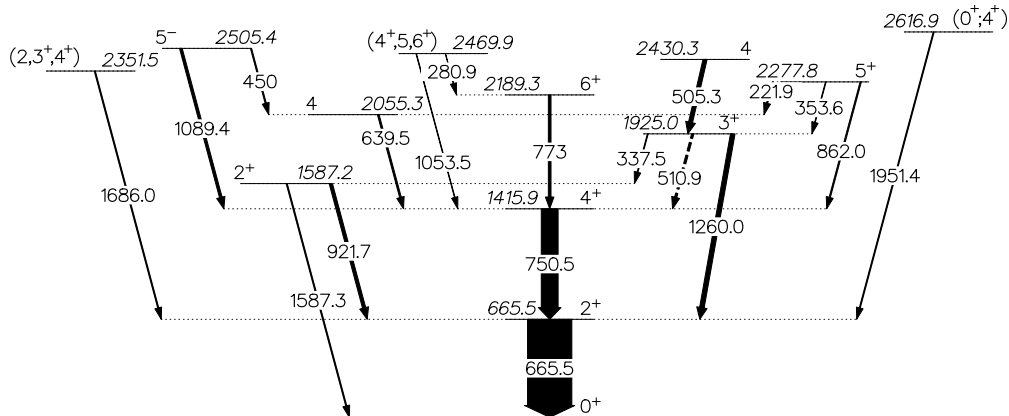


FIG. 2. The  $^{100}\text{Pd}$  low-energy level scheme and the relevant  $\gamma$ -ray transitions observed in this experiment. The widths of the transition arrows are proportional to the observed intensities. All energies are in keV.

Figure 2 presents the partial level scheme of  $^{100}\text{Pd}$ , based on the  $\gamma$ -ray transitions observed in this experiment, and constructed from the  $\gamma$ - $\gamma$  and the particle- $\gamma$  coincidence matrices. This level scheme is in agreement with recent results by Radeck *et al.* [4]. Figure 3 displays different particle projections from the particle- $\gamma$  coincidence matrix. The peaks labeled 1 and 2 (Fig. 3b) correspond to the detection of one and two  $\alpha$  particles respectively, while the broad high energy peak (Fig. 3c) corresponds to carbon nuclei scattered in the Coulomb excitation process. Figure 4 shows the cleanest  $^{100}\text{Pd}$   $\gamma$ -ray spectrum obtained by setting a particle gate on the two- $\alpha$  peak.

#### 4. Measurement of the precession angle, $\Delta\theta^{exp}$

The measured precession angle,  $\Delta\theta^{exp} = \epsilon^{exp}/S(\theta_\gamma)^{exp}$  [12], is given by the ratio of the precession effect ( $\epsilon^{exp}$ ) to the logarithmic slope ( $S(\theta_\gamma)^{exp}$ ) of the angular correlation of the gamma radiation evaluated at the angle  $\theta_\gamma$ ,

$$S(\theta_\gamma)^{exp} = \frac{1}{W(\theta_\gamma)} \cdot \left. \frac{dW(\theta)}{d\theta} \right|_{\theta=\theta_\gamma}, \quad (1)$$

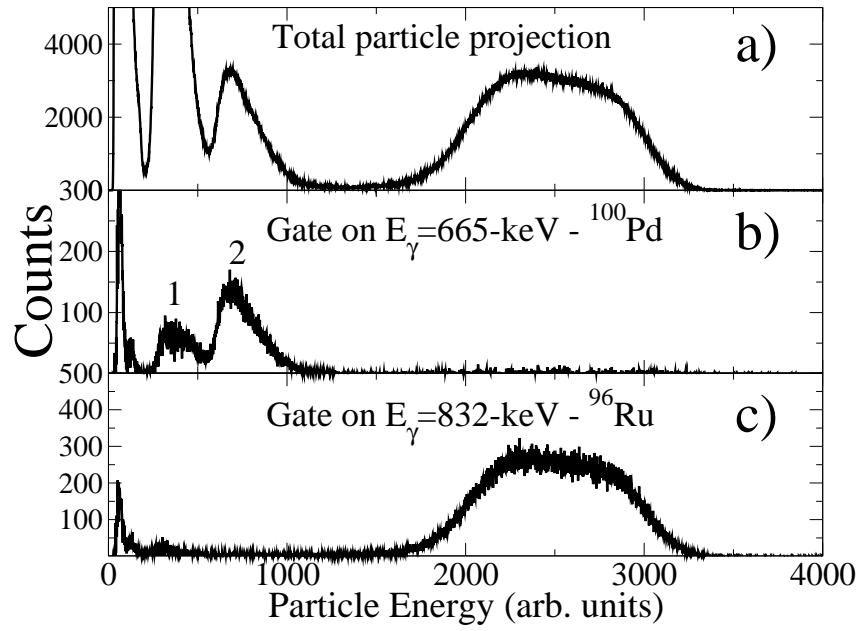


FIG. 3. Particle spectra: a) total particle projection from the  $\gamma$ -particle coincidence matrix; b) gated on the  $2_1^+ \rightarrow 0_1^+$   $\gamma$ -ray transition of  $^{100}\text{Pd}$ ; and c) gated on the  $2_1^+ \rightarrow 0_1^+$   $\gamma$ -ray transition of  $^{96}\text{Ru}$ .

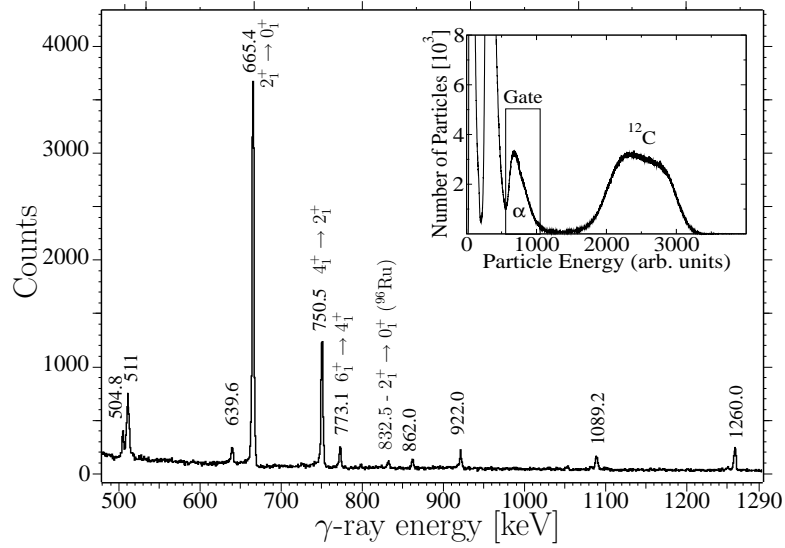


FIG. 4. The  $\gamma$ -ray spectrum, from clover 1, in coincidence with  $\alpha$  particles. Simultaneous signals from neighboring crystals were added (Compton add-back). The gate on the  $\alpha$  particles is shown in the upper-right corner of the spectrum. The  $\gamma$  spectrum is dominated by the  $2_1^+ \rightarrow 0_1^+$  and  $4_1^+ \rightarrow 2_1^+$  transitions.

where the angle  $\theta_\gamma$  is measured with respect to the beam axis, and is determined in the rest frame of the  $\gamma$ -emitting nuclei. The particle- $\gamma$  ray angular correlation function is given by [20, 21]

$$W(\theta) = 1 + A_2 \cdot Q_2 \cdot P_2(\cos \theta) + A_4 \cdot Q_4 \cdot P_4(\cos \theta). \quad (2)$$

Here the  $P_k(\cos \theta)$  are Legendre polynomials of degree  $k$ , the  $A_k$  are the angular-correlation coefficients which depend on the multipolarity of the  $\gamma$ -ray transition, and the  $Q_k$  are the geometrical attenuation coefficients. The angular correlation coefficients can be determined from the precession data [22]. Anisotropy data were derived from the individual Ge crystals inside the clover detectors. The latter approach enables the use of the full statistics of the precession data. However, the angle  $\theta$  in Eq. (2) is evaluated at two values ( $67^\circ \pm 8^\circ$ , where  $8^\circ$  is the separation angle of the clover segments).

Nevertheless, an independent angular correlation measurement was carried out in a separate experiment to extend the angular range and to confirm the logarithmic slope. This experiment used a  $^{96}\text{Ru}$  beam of 340 MeV, with a different multilayered target consisting of  $0.45 \text{ mg/cm}^2$  of carbon, deposited on  $4.16 \text{ mg/cm}^2$  of iron, backed by  $5.49 \text{ mg/cm}^2$  of copper. The clover detectors 1 and 2 were kept stationary and used for normalization, while clovers 3 and 4 were moved through a range of angles in steps of 5 and 10 degrees. The measured intensities of the  $2_1^+ \rightarrow 0_1^+$  transition in clovers 3 and 4, after correcting for the relative efficiencies, are shown in Fig. 5.

The logarithmic slopes from the two experiments agree with each other and were combined for the calculation of the precession angle. In  $^{100}\text{Pd}$  small  $S(67^\circ)^{exp}$  values of  $-0.32(5)$  and  $-0.55(4)$  were obtained for the  $2_1^+ \rightarrow 0_1^+$  and the  $4_1^+ \rightarrow 2_1^+$  transitions, respectively. In contrast, for  $^{96}\text{Ru}$ , a value of  $S(67^\circ)^{exp} = -1.85(5)$  was measured for the  $2_1^+ \rightarrow 0_1^+$   $\gamma$ -ray transition in the latter independent angular correlation measurement. It is noted that the measured slopes for the  $\alpha$ -transfer channel that were obtained in the present investigation are similar to the corresponding data obtained by the Bonn group for several other nuclei [7–10].

The slope for the  $4_1^+$  state has a larger value than the slope for the  $2_1^+$  state. This characteristic has been observed not only in previous work on  $\alpha$ -transfer reactions [9], but also on fusion-evaporation reactions [9, 23–25]. In contrast, Coulomb excitation reactions exhibit a lower slope for the  $4_1^+$  state than for the  $2_1^+$  state [1, 22, 26–29]. The population mechanism for alpha-transfer (and fusion-evaporation) reactions may be responsible for the increase of the slope with spin. Future studies should clarify the origin of this difference.

Figure 5 shows the comparison, between  $^{100}\text{Pd}$  and  $^{96}\text{Ru}$ , of the experimental  $\gamma$ -ray angular correlations for the  $2_1^+ \rightarrow 0_1^+$  transitions. The results of the corresponding fits to the  $A_k$  coefficients in Eq. (2) are displayed there as solid and dashed curves, respectively. The Coulomb-excitation channel ( $^{96}\text{Ru}$ ) provides a more pronounced  $\gamma$ -ray angular

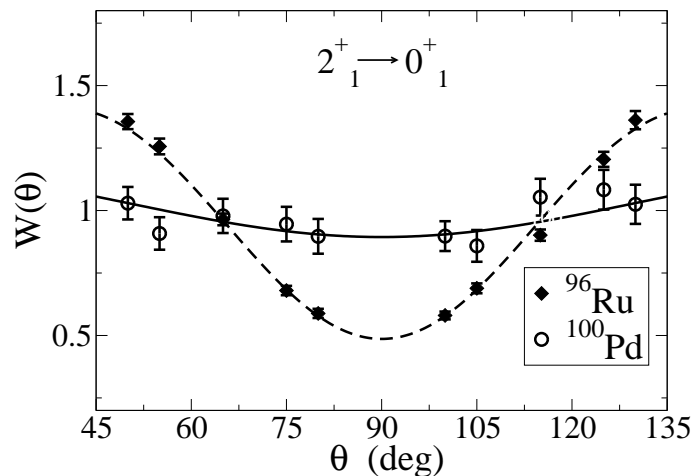


FIG. 5. The experimental  $\gamma$ -ray angular correlations,  $W(\theta)$ , for the  $2_1^+ \rightarrow 0_1^+$  transitions; open circles correspond to  $^{100}\text{Pd}$  and diamonds to  $^{96}\text{Ru}$ . The solid and dashed lines correspond to fits to the angular correlation function for  $^{100}\text{Pd}$  and  $^{96}\text{Ru}$ , respectively (see text for details).

correlation pattern than does the  $\alpha$ -transfer channel ( $^{100}\text{Pd}$ ), indicating a larger spin alignment for the Coulomb excitation reaction.

The measured precession effect [12],  $\epsilon^{exp} = (\rho - 1)/(\rho + 1)$ , is calculated from quadruple ratios involving the four HP-Ge clover detectors:

$$\rho = \sqrt{\rho_{1,4}/\rho_{2,3}} \quad \text{with} \quad \rho_{i,j} = \sqrt{(N_i^\uparrow \cdot N_j^\downarrow)/(N_i^\downarrow \cdot N_j^\uparrow)}, \quad (3)$$

where  $N_i^\uparrow$  ( $N_i^\downarrow$ ) is the  $\gamma$ -ray peak intensity that is measured in clover  $i$  when the external magnetic field,  $B_{ext}$ , is up (down) with respect to the particle- $\gamma$  scattering plane.

### 5. Calculation of the corrections to $\epsilon^{exp}$ and $S(\theta_\gamma)^{exp}$

A given nuclear state which is *directly* populated during the nuclear reaction, and whose magnetic moment precesses while the nucleus is in that same state, is characterized by a precession angle denoted by  $\Delta\theta_{dir}$ . In this work such a state will be denoted as a “directly populated state”. However, during the  $\alpha$ -transfer process the excited states are not only populated directly, but are also fed from decaying feeding states. Thus, the measured precession angle, denoted by  $\Delta\theta^{exp}$ , reflects the precession of the magnetic moment of the state of interest as well as the precession of the magnetic moments of higher-energy states. To determine  $\Delta\theta^{dir} = \epsilon_{dir}/S(67^\circ)_{dir}$ , the quantities  $\epsilon_{dir}$  and  $S(67^\circ)_{dir}$

need to be extracted from  $\epsilon^{exp}$  and  $S(67^\circ)^{exp}$  using [27, 29–31]

$$\epsilon^{exp} = \frac{\epsilon_{dir}N_{dir} + \sum_k \epsilon_k N_k}{N_{dir} + \sum_k N_k}, \quad \text{and} \quad S^{exp} = \frac{S_{dir}N_{dir} + \sum_k S_k N_k}{N_{dir} + \sum_k N_k}, \quad (4)$$

where  $k$  accounts for contributions from all the other states that are feeding the state of interest. The quantities  $\epsilon$ 's,  $S$ 's, and  $N$ 's are, respectively, the values of the precession effects, logarithmic slopes, and efficiency-corrected photopeak intensities. The quantity  $N_{total} = N_{dir} + \sum_k N_k$  is the total observed photopeak intensity of the transition under study (see Table I), where  $N_{dir}$  is the directly populated photopeak intensity, while the  $N_k$ 's represent the photopeak intensities of the feeding transitions. The use of Eq. (4), to estimate  $\Delta\theta_{dir}$ , requires a detailed knowledge of the states' spin precession ( $\epsilon_k$ 's), transition intensities ( $N_k$ 's), and the logarithmic slopes ( $S_k$ 's) of the transitions feeding the state under study. In this experiment the required spectroscopic information was neither complete nor precise. In particular, the corrected slopes,  $S(67^\circ)_{dir}$ , could not be evaluated reliably; hence  $S(67^\circ)^{exp}$  was used throughout to evaluate the precession  $\Delta\theta_{dir}$ .

## 6. Calculation of $g$

The  $g$  factor for each state is calculated using the formula

$$\Delta\theta_{dir} = -g \cdot \frac{\mu_N}{\hbar} \cdot \int_{t_{in}}^{t_{out}} B_{TF}(v(t), Z) \cdot e^{-t/\tau} dt. \quad (5)$$

Here  $\mu_N$  is the nuclear magneton ( $e\hbar/2M_p c$ ),  $t_{in}$  ( $t_{out}$ ) is the mean entrance (exit) time of the ions into the ferromagnetic gadolinium layer,  $\tau$  is the mean lifetime of the state being considered, and  $B_{TF}$  is the transient magnetic field calculated using the Rutgers parametrization [32],

$$B_{TF}(v(t), Z) = a \cdot Z^{1.1} \cdot \left(\frac{v}{v_0}\right)^{0.45} \cdot M \quad . \quad (6)$$

Above,  $a = 96.7 \pm 1.6$  is the strength parameter,  $v_0 = c/137$  is the Bohr velocity, and  $M$  is the magnetization of the target in tesla. The use of Eq. (5) to obtain the  $g$  factor requires the evaluation of  $\Delta\theta_{dir}$  and the calculation of the integral  $\Delta\theta(g=1) = -\mu_N/\hbar \cdot \int B_{TF} \cdot e^{-t/\tau} dt$ . Thus, the  $g$  factor becomes

$$g = \frac{\Delta\theta_{dir}}{\Delta\theta(g=1)} \quad . \quad (7)$$

For the evaluation of  $\Delta\theta(g=1)$  the program **gfac** from Rutgers University was utilized. The code **gfac** uses as input the parameters of Eqs. (5) and (6) for the calculation of  $\Delta\theta(g=1)$ . The calculations of the energy loss within the target for the  $^{12}\text{C}$  ions and for the  $^{100}\text{Pd}$  nuclei were based on the stopping powers of Ref. [33]. The

initial and final energies of the  $^{100}\text{Pd}$  ions, entering and leaving the gadolinium foil, were estimated to be 213.8 MeV and 78.6 MeV, corresponding to a velocity range of  $\langle v/v_0 \rangle_{\text{in}} = 9.29$  to  $\langle v/v_0 \rangle_{\text{out}} = 5.63$ . The calculated values  $\Delta\theta(2_1^+; g = 1) = 67.4$  mrad and  $\Delta\theta(4_1^+; g = 1) = 63.8$  mrad were used in the evaluation of the  $g$  factors.

In this experiment an automatic check of the procedure is provided by the simultaneous Coulomb excitation of the  $^{96}\text{Ru}$  beam. A value of  $g(^{96}\text{Ru}; 2_1^+) = +0.46(3)$  was obtained, in agreement with the value  $g(2_1^+) = +0.47(3)$  reported

TABLE I. The  $\gamma$ -ray transitions observed in the present work (at a beam energy of 350 MeV). The photopeak intensities ( $N_\gamma$ ) are normalized to the  $2_1^+ \rightarrow 0_1^+$   $\gamma$ -ray intensity, whose value is arbitrarily set to 100. The intensities do not take into account the angular correlation of the  $\gamma$ -ray radiation because of the small alignment of the states.

Level Energy	Transition	$\gamma$ -ray energy	Intensity
$E_i$ [keV]	$J_i^\pi \rightarrow J_f^{\pi\text{a}}$	$E_\gamma$ [keV]	$N_\gamma$
665.51(21)	$2_1^+ \rightarrow 0_1^+$	665.50(10)	100
1415.9(4)	$4_1^+ \rightarrow 2_1^+$	750.50(20)	38.0(5)
1587.2(3)	$2_2^+ \rightarrow 2_1^+$	921.70(10)	7.3(3)
	$2_2^+ \rightarrow 0_1^+$	1587.3(3)	2.4(2)
1925.0(5)	$3_1^+ \rightarrow 2_2^+$	337.5(3)	1.80(20)
	$3_1^+ \rightarrow 4_1^+$	510.9(4)	$< 7^{\text{a}}$
	$3_1^+ \rightarrow 2_1^+$	1260.0(6)	10.3(3)
2055.3(6)	$4 \rightarrow 4_1^+$	639.5(10)	3.80(21)
2189.3(6)	$6_1^+ \rightarrow 4_1^+$	773.0(7)	6.0(2)
2277.8(6)	$5_1^+ \rightarrow 4$	221.9(3)	2.5(3)
	$5_1^+ \rightarrow 3_1^+$	353.6(5)	1.4(2)
	$5_1^+ \rightarrow 4_1^+$	862.0(2)	2.80(18)
2351.5(18)	$(2, 3^+, 4^+) \rightarrow 2_1^+$	1686.0(8)	2.4(2)
2430.3(6)	$4 \rightarrow 3_1^+$	505.30(10)	9.1(3)
2469.9(7)	$(4^+, 5, 6^+) \rightarrow 6_1^+$	280.90(20)	0.60(14)
	$(4^+, 5, 6^+) \rightarrow 4_1^+$	1053.5(3)	1.23(17)
2505.4(5)	$5_1^- \rightarrow 4$	450.4(3)	2.6(3)
	$5_1^- \rightarrow 4_1^+$	1089.40(10)	6.0(3)
2616.9(7)	$(0^+, 4^+) \rightarrow 2_1^+$	1951.4(3)	2.20(20)

<sup>a</sup> Assignment taken from Ref. [4].

TABLE II. Experimental and corrected effects  $\epsilon$  and precession  $\Delta\theta$  values. The quantities  $\epsilon^{exp}$ ,  $S^{exp}$  and  $\Delta\theta^{exp}$  refer to the precession effects, the logarithmic slopes and the precession angles obtained without any feeding correction. The quantities  $\epsilon_{dir}$ ,  $\Delta\theta_{dir}$  and  $g$  include the feeding corrections to  $\epsilon_{exp}$ . The errors quoted in the  $g$  factors reported in the last column stem mainly from the statistical errors in  $\epsilon^{exp}$  and do not include the propagated errors arising from the feeding (see text).

$E_i$ [keV]	$J_i^\pi$	$\tau$ [ps] <sup>a</sup>	$\epsilon^{exp}$	$S(67^\circ)^{exp}$ [rad <sup>-1</sup> ]	$\Delta\theta^{exp}$ [mrad]	$g_{exp}$	$\epsilon_{dir}$	$\Delta\theta_{dir}$ [mrad]	$g$
665.5	$2_1^+$	9.0(4)	-0.0086(36)	-0.324(54)	+26.5(120)	+0.39(18)	-0.0066(28)	+20.4(92)	+0.30(14)
1415.9	$4_1^+$	3.6(3)	-0.0157(49)	-0.550(39)	+28.5(91)	+0.45(14)	-0.0156(49)	+28.4(91)	+0.45(14)
2189.3	$6_1^+$	3.7(5)	-0.0517(267)	-0.547(156)	+94.5(558)	+1.47(87)			

<sup>a</sup> Lifetimes taken from Ref. [6].

in Ref. [34].

### III. EXPERIMENTAL RESULTS

Table II displays the experimental results of the present work. The superscript “*exp*” refers to the measured values. The  $g_{exp}$  values correspond to the experimental  $g$  factors, calculated from the precession angle,  $\Delta\theta^{exp}$ , and do not take into account feeding corrections. The quantity  $\Delta\theta_{dir}$  refers to the precession of the “directly-populated” state, obtained after the correction described in section II 5 was applied.

For all the  $\gamma$ -ray transitions with energies larger than 780 keV, a combined precession value of  $\epsilon^{exp} \sim 0$  was measured, probably due to the small spin alignment. Hence, contributions to the corrections from those states in Eq. (4) are small and were neglected for both the  $2_1^+$  and the  $4_1^+$  states, but they were included in the intensity balance of Eq. (4). The  $g$  factors reported in the last column of Table II take into account only the correction to  $\epsilon^{exp}$ , the precession effect of Eq. (4). The feeding corrections have practically no effect on the magnitude of the resulting  $g$  factors for either the  $2_1^+$  or the  $4_1^+$  states. This result follows directly from the nearly equal measured precessions, bearing in mind that the main feeding component of the  $2_1^+$  state comes from the  $4_1^+$  state. However, because the errors in the correction terms are themselves poorly determined, the procedure greatly amplifies the errors, yielding  $\epsilon_{dir}(2_1^+) = -0.0066(114)$  and  $\epsilon_{dir}(4_1^+) = -0.0156(134)$ , which correspond to  $g(2_1^+) = +0.30(52)$  and  $g(4_1^+) = +0.45(38)$  respectively. Hence, for a more constrained comparison with theoretical predictions, the final  $g$  factors are quoted with only the statistical errors in  $\epsilon^{exp}$  included.

The  $6_1^+$  does not require any feeding corrections. Due to its low excitation the derived  $g$  factor has a large uncertainty and is therefore not discussed further.

#### IV. SHELL MODEL AND COLLECTIVE MODEL PERSPECTIVES

In order to investigate the structure of  $^{100}\text{Pd}$ , large-scale Shell-Model (SM) calculations were performed using the Oslo code [35]. In these calculations  $^{88}\text{Sr}$  was taken as the inert core, and the effective interaction was constructed based on the CD-Bonn nucleon-nucleon interaction described in Ref. [35]. The model space for the valence nucleons included the  $\pi$  orbitals ( $1p_{1/2}$ ,  $0g_{9/2}$ ), and the  $\nu$  orbitals ( $1d_{5/2}$ ,  $0g_{7/2}$ ,  $1d_{3/2}$ ,  $2s_{1/2}$ ,  $0h_{11/2}$ ). The Single-Particle Energies (SPE) relative to a  $^{88}\text{Sr}$  core, were taken from Refs. [4, 6]. There, the SPE were deduced from the experimental data on excited states and on proton and neutron separation energies in the one-valence-nucleon neighbours of the core, i.e.  $^{89}\text{Y}$  and  $^{89}\text{Sr}$ . The resulting SPE, utilized in the calculations, were:  $\epsilon_\pi(1p_{1/2}) = -6.160$  MeV,  $\epsilon_\pi(0g_{9/2}) = -7.069$  MeV,  $\epsilon_\nu(1d_{5/2}) = -6.359$  MeV,  $\epsilon_\nu(0g_{7/2}) = -3.684$  MeV,  $\epsilon_\nu(1d_{3/2}) = -4.351$  MeV,  $\epsilon_\nu(2s_{1/2}) = -5.327$  MeV,  $\epsilon_\nu(0h_{11/2}) = -4.280$  MeV. These calculations used the free-nucleon  $g$  factors for protons and neutrons ( $g_l' = 0.0$ ,  $g_s' = -3.8263$ ,  $g_l^\pi = 1.0$ , and  $g_s^\pi = 5.5855$ ), and the effective charges  $\epsilon_\nu = 1.0e$  and  $\epsilon_\pi = 1.7e$  (see Ref. [6]).

Other different effective values for the nucleon  $g$  factors were also tried out to study their effects on the calculated results. These studies showed that the  $g$  factors of the states in  $^{100}\text{Pd}$  are more sensitive to changes in the orbital than in the spin nucleon  $g$  factors. For example, increasing the  $g_l'$  and  $g_l^\pi$  by adding 0.2 to each of them, increase the  $g(2_1^+)$  and  $g(4_1^+)$  by over 30%. On the other hand, decreasing the magnitudes of  $g_s'$  and  $g_s^\pi$  by 30% each, decreases the  $g(2_1^+)$  and the  $g(4_1^+)$  values only by about 10%.

Table III shows the results for  $^{100}\text{Pd}$  of the large-scale SM calculations for the excitation energies, transition

TABLE III. Comparison between the results of the large-scale shell model calculations (SM) and the experimental (*exp*) quantities for the two lowest excited states energies and transitions under study in  $^{100}\text{Pd}$ .

State		$E_x(J_i^\pi)$ [keV]		$B(E2 : J_i^\pi \rightarrow J_f^\pi)$ [W.u.]		$g(J_i^+)$	
$J_i^\pi$	$J_f^\pi$	<i>exp</i>	SM	<i>exp</i>	SM <sup>a</sup>	<i>exp</i> <sup>b</sup>	SM
$2_1^+$	$0_1^+$	665.4	751.9	25.4(11)	21.8	+0.30(14)	+0.78
$4_1^+$	$2_1^+$	1416.1	1507.1	35(3)	30.0	+0.45(14)	+0.66

<sup>a</sup> Using the effective charges:  $\epsilon_\nu = 1.0e$  and  $\epsilon_\pi = 1.7e$  from Ref. [4].

<sup>b</sup> Values from this work.

strengths, and  $g$  factors.

The average occupation numbers obtained in the SM calculations are shown in Table IV, for the  $0_1^+$ ,  $2_1^+$  and  $4_1^+$  states of  $^{100}\text{Pd}$ . The proton occupations for these states range from 3.35 to 3.67 proton holes in the  $0g_{9/2}$  orbital, and from 1.35 to 1.67 proton particles in the  $1p_{1/2}$  orbital. Of the four valence neutrons beyond  $N = 50$ , the two  $0g_{7/2}$  and  $1d_{5/2}$  orbitals were occupied by between 3.16 and 3.28 neutrons.

The calculated level-excitation energies are only slightly larger than the experimental ones, by about 90 keV. The calculated transition strengths  $B(E2; 2_1^+ \rightarrow 0_1^+)$  and  $B(E2; 4_1^+ \rightarrow 2_1^+)$  are in good agreement with the experimental values reported by Radeck et al. in Ref. [6]. The above agreements suggest that the shell model picture is an appropriate one for the low-lying levels of  $^{100}\text{Pd}$ . On the whole, the calculations lead to results that are similar to those obtained in [4, 6, 36] although a different interaction and a different computer code were used. Ref [4, 6], however, did not consider  $g$  factors.

The measured  $g$  factors are smaller than the calculated shell-model  $g_{SM}$  values for the  $2_1^+$  and  $4_1^+$  states. The large positive  $g_{SM}$  values may perhaps be related to the partial occupation of the  $0g_{9/2}$  orbital by protons (the Schmidt value for the  $g_{9/2}$  protons is +1.510), or to an underestimation of the contributions of the neutrons to the wave functions.

Shell model calculations were also carried out with smaller shell-model spaces. The results suggest that the exclusion of the  $\nu(h_{11/2})$  orbital would have only a small effect on the calculated values for  $^{100}\text{Pd}$ . Indeed, the average occupation number of this orbital is only about 0.1 neutrons (see Table IV). On the other hand, all the other orbitals (of both protons and neutrons) have to be included in the shell model space in order to obtain a good approximation to the experimental  $B(E2)$  values in  $^{100}\text{Pd}$ .

As noted in the Introduction, collective models have also been applied to the  $^{100}\text{Pd}$  nucleus. It was pointed out there that the measured excitation-energy ratios ( $R_{4/2} = 2.13$  and  $R_{6/2} = 3.29$ ) are close to the vibrational

TABLE IV. Shell model results for the average nucleon occupation numbers, for the orbitals under consideration, for the  $0_1^+$ ,  $2_1^+$ , and  $4_1^+$  states in  $^{100}\text{Pd}$ .  $E_x$  refers to the calculated level excitation energy.

$J_i^\pi$	$E_x$ [keV]	$\pi$		$\nu$				
		$0g_{9/2}$	$1p_{1/2}$	$0h_{11/2}$	$0g_{7/2}$	$1d_{5/2}$	$1d_{3/2}$	$2s_{1/2}$
$0_1^+$	0.0	6.65	1.35	0.12	1.47	1.81	0.37	0.24
$2_1^+$	752	6.49	1.51	0.08	1.39	1.77	0.43	0.33
$4_1^+$	1507	6.33	1.67	0.06	1.44	1.74	0.46	0.30

model predictions ( $R_{4/2} = 2$  and  $R_{6/2} = 3$ ). The experimental  $B(E2 : 4_1^+ \rightarrow 2_1^+)$  and  $B(E2 : 2_1^+ \rightarrow 0_1^+)$  (see Table III) show collective enhancements consistent with the vibrational picture. However, the experimental ratio  $B(E2 : 4_1^+ \rightarrow 2_1^+)/B(E2 : 2_1^+ \rightarrow 0_1^+) = 1.38(17)$  is lower than the vibrational prediction of 2.0.

In Ref. [4] no  $0_2^+$  was found near the  $2_2^+$  and  $4_1^+$  states. The lowest possible  $0_2^+$  state there lies close to 1 MeV higher. In the shell model calculations for  $^{100}\text{Pd}$  the excitation energies of these three states differ by only about 260 keV. Generally speaking, the even Pd isotopes beyond the semi-magic  $^{96}\text{Pd}$  (with 50 neutrons) gradually become more collective as the neutron number increases. The measured excitation energies of the  $0_2^+$ ,  $2_2^+$ , and  $4_1^+$  states differ by 320 keV for  $^{102}\text{Pd}$ , but by no more than 130 keV for all the heavier even Pd isotopes. The experimental  $E(2_1^+)$  excitation energy (665 keV for  $^{100}\text{Pd}$ ) decreases monotonically from 1453 keV in  $^{96}\text{Pd}$  to 373.8 keV in  $^{110}\text{Pd}$ .

The resulting  $g(4_1^+) = +0.45(14)$  agrees, within error, with the simple collective model prediction of  $g_{collective} = Z/A = +0.46$  for all the states. The  $g(2_1^+) = +0.30(14)$  comes close to such an agreement. In Ref. [5] a collective IBA-2 calculation yielded  $g(2_1^+) = 0.40$  and it was noted that additional experimental results are required to clarify the relative amounts of U(5) and O(6) collectivity, and to clearly find the position of  $^{100}\text{Pd}$  in the Casten triangle. The collective model prediction of  $g(4_1^+) = g(2_1^+)$  is consistent with the present results within the errors, but the data still suggest that  $g(4_1^+) > g(2_1^+)$ . Further experimental work is needed to determine  $g$  factors with greater accuracy to clarify this point.

## V. SUMMARY

The  $g$  factors of the  $2_1^+$  and  $4_1^+$  excited states in the radioactive  $^{100}\text{Pd}$  nucleus were studied using  $\alpha$ -transfer reactions, in combination with the transient-field technique in inverse kinematics. Large-scale shell-model calculations provide results that account well for the measured excitation energies, and the  $B(E2)$  values, but overestimate the  $g$  factors. The measured  $g$  factors are consistent, within the errors, with a collective model picture.

The use of  $\alpha$ -transfer reactions in inverse kinematics, in combination with the transient field technique, offers the possibility to study magnetic moments of low-spin states of nuclei which, otherwise, will be difficult to investigate with the present available beam facilities. Future radioactive beam facilities will permit the study of these nuclei, such as  $^{100}\text{Pd}$ , using Coulomb-excitation reactions.

The production of significant excitation yields and of states with considerable spin alignment is fundamental for measuring  $g$  factors. The  $\alpha$ -transfer reaction tends to populate low-lying low-spin states, both directly and by feeding from populated higher states. The spin alignment and the relative role of direct population increase slightly with the

excitation energy. The spin alignment is smaller than in Coulomb excitation reactions, but valuable results can still be obtained. Higher-lying states are also excited in the  $\alpha$ -transfer reaction. As was mentioned in the Introduction, the use of  $\alpha$ -transfer reactions, for measuring  $g$  factors, in the  $A < 70$  mass region, has been successfully implemented. For heavier nuclei, and for larger level densities, the calculations of feeding corrections present a serious challenge. Detailed spectroscopic information for the populated states is necessary to estimate the corrections to the  $g$  factors.

It will be valuable to carry out future experimental and theoretical studies of the  $\alpha$ -transfer reaction. Specifically, such studies should investigate the reaction mechanism, the decay history of the states populated by the reaction, and the particle- $\gamma$  angular correlations. These investigations could reduce the experimental uncertainties, and help to extend the use of the  $\alpha$ -transfer technique to higher mass regions and to nuclei with larger level densities.

## VI. ACKNOWLEDGMENTS

The authors are indebted to the staff of the Wright Nuclear Structure Laboratory for their assistance during the experiment. The work was supported in part by the US National Science Foundation and the US Department of Energy under Grant DE-FG02-91ER-40609. Y.Y.S. would like to acknowledge a Stockton College Research and Professional Development Grant. D.A.T would like to thank Fernando Cristancho for stimulating discussions, and the Universidad Nacional de Colombia and the Centro Internacional de Física for hosting him as a guest researcher. K.H.S acknowledges support by the DFG under SP 190/16-1. D.R. and D.S. acknowledges support by the German Academic Exchange Service (DAAD).

- 
- [1] G. Gürdal, G. J. Kumbartzki, N. Benczer-Koller, Y. Y. Sharon, L. Zamick, S. J. Q. Robinson, T. Ahn, R. Casperson, A. Heinz, G. Ilie, J. Qian, V. Werner, E. Williams, R. Winkler, and D. McCarthy, *Phys. Rev. C* **82**, 064301 (2010).
  - [2] A. Dewald, K. Starosta, P. Petkov, M. Hackstein, W. Rother, P. Adrich, A. M. Amthor, T. Baumann, D. Bazin, M. Bowen, A. Chester, A. Dunomes, A. Gade, D. Galaviz, T. Glasmacher, T. Ginter, M. Hausmann, J. Jolie, B. Melon, D. Miller, V. Moeller, R. P. Norris, T. Pissulla, M. Portillo, Y. Shimbara, A. Stolz, C. Vaman, P. Voss, and D. Weisshaar, *Phys. Rev. C* **78**, 051302 (2008).
  - [3] N. V. Zamfir, M. A. Caprio, R. F. Casten, C. J. Barton, C. W. Beausang, Z. Berant, D. S. Brenner, W. T. Chou, J. R. Cooper, A. A. Hecht, R. Krücken, H. Newman, J. R. Novak, N. Pietralla, A. Wolf, and K. E. Zyromski, *Phys. Rev. C* **65**, 044325 (2002).

- [4] D. Radeck, M. Albers, C. Bernards, L. Bettermann, A. Blazhev, C. Fransen, S. Heinze, J. Jolie, and D. MÜcher, *Nuclear Physics A* **821**, 1 (2009).
- [5] M. Sambataro and A. E. L. Dieperink, *Physics Letters B* **107**, 249 (1981).
- [6] D. Radeck, A. Blazhev, M. Albers, C. Bernards, A. Dewald, C. Fransen, M. Heidemann, J. Jolie, B. Melon, D. MÜcher, T. Pissulla, W. Rother, K. O. Zell, and O. Möller, *Phys. Rev. C* **80**, 044331 (2009).
- [7] S. Schielke, K.-H. Speidel, O. Kenn, J. Leske, N. Gemein, M. Offer, Y. Y. Sharon, L. Zamick, J. Gerber, and P. Maier-Komor, *Physics Letters B* **567**, 153 (2003).
- [8] K.-H. Speidel, S. Schielke, J. Leske, J. Gerber, P. Maier-Komor, S. Robinson, Y. Y. Sharon, and L. Zamick, *Physics Letters B* **632**, 207 (2006).
- [9] K.-H. Speidel, J. Leske, S. Schielke, S. Bedi, O. Zell, P. Maier-Komor, S. Robinson, Y. Y. Sharon, and L. Zamick, *Physics Letters B* **633**, 219 (2006).
- [10] J. Leske, K.-H. Speidel, S. Schielke, O. Kenn, J. Gerber, P. Maier-Komor, S. J. Q. Robinson, A. Escuderos, Y. Y. Sharon, and L. Zamick, *Phys. Rev. C* **71**, 044316 (2005).
- [11] D.A. Torres et al., to be published.
- [12] N. Benczer-Koller and G. J. Kumbartzki, *Journal of Physics G: Nuclear and Particle Physics* **34**, R321 (2007).
- [13] P. Maier-Komor, K. Speidel, and A. Stolarz, *Nuclear Instruments and Methods in Physics Research Section A: Accelerators, Spectrometers, Detectors and Associated Equipment* **334**, 191 (1993).
- [14] E. Mathiak, K. A. Eberhard, J. G. Cramer, H. H. Rossner, J. Stettmeier, and A. Weidinger, *Nuclear Physics A* **259**, 129 (1976).
- [15] A. Piqué, J. Brennan, R. Darling, R. Tanczyn, D. Ballon, and N. Benczer-Koller, *Nuclear Instruments and Methods in Physics Research Section A: Accelerators, Spectrometers, Detectors and Associated Equipment* **279**, 579 (1989).
- [16] Canberra, “Ge clover detectors,” <http://www.canberra.com/products/1112.asp>.
- [17] X-Ray Instrumentation Associates, <http://www.xia.com/>.
- [18] G. Kumbartzki, “Program XSA,” <http://www.physics.rutgers.edu/~kum/>.
- [19] J. Theuerkauf, S. Esser, S. Krink, M. Luig, N. Nicolay, O. Stuch, and H. Wolters, program Tv, University of Cologne, unpublished.
- [20] R. Gill, in *Gamma Ray Angular Correlations* (New York: Academic Press, 1975).
- [21] K. Alder and A. Winther, in *Electromagnetic Excitations* (Amsterdam: North-Holland, 1975).
- [22] P. Boutachkov, S. J. Q. Robinson, A. Escuderos, G. Kumbartzki, N. Benczer-Koller, E. Stefanova, Y. Y. Sharon, L. Zamick, E. A. McCutchan, V. Werner, H. Ai, A. B. Garnsworthy, G. Gürdal, A. Heinz, J. Qian, N. J. Thompson, E. Williams, and R. Winkler, *Phys. Rev. C* **76**, 054311 (2007).
- [23] A. W. Mountford, J. Billowes, W. Gelletly, H. G. Price, and D. D. Warner, *Physics Letters B* **279**, 228 (1992).

- [24] A. I. Kucharska, J. Billowes, and C. J. Lister, *Journal of Physics G: Nuclear and Particle Physics* **15**, 1039 (1989).
- [25] A. Stuchbery, C. Ryan, H. Bolotin, I. Morrison, and S. Sie, *Nuclear Physics A* **365**, 317 (1981).
- [26] A. E. Stuchbery, C. G. Ryan, H. H. Bolotin, and S. H. Sie, *Phys. Rev. C* **23**, 1618 (1981).
- [27] K.-H. Speidel, N. Benczer-Koller, G. Kumbartzki, C. Barton, A. Gelberg, J. Holden, G. Jakob, N. Matt, R. H. Mayer, M. Satteson, R. Tanczyn, and L. Weissman, *Phys. Rev. C* **57**, 2181 (1998).
- [28] R. Ernst, K.-H. Speidel, O. Kenn, A. Gohla, U. Nachum, J. Gerber, P. Maier-Komor, N. Benczer-Koller, G. Kumbartzki, G. Jakob, L. Zamick, and F. Nowacki, *Phys. Rev. C* **62**, 024305 (2000).
- [29] T. J. Mertzimekis, N. Benczer-Koller, J. Holden, G. Jakob, G. Kumbartzki, K.-H. Speidel, R. Ernst, A. Macchiavelli, M. McMahan, L. Phair, P. Maier-Komor, A. Pakou, S. Vincent, and W. Korten, *Phys. Rev. C* **64**, 024314 (2001).
- [30] D. Ballon, Y. Niv, S. Vajda, N. Benczer-Koller, L. Zamick, and G. A. Leander, *Phys. Rev. C* **33**, 1461 (1986).
- [31] A. E. Stuchbery, I. Morrison, L. D. Wood, R. A. Bark, H. Yamada, and H. H. Bolotin, *Nuclear Physics A* **435**, 635 (1985).
- [32] N. K. B. Shu, D. Melnik, J. M. Brennan, W. Semmler, and N. Benczer-Koller, *Phys. Rev. C* **21**, 1828 (1980).
- [33] F. Ziegler, J. Biersack, and U. Littmark, in *The Stopping and Range of Ions in Solid*, Vol. 1 (Pergamon, Oxford, 1985).
- [34] M. J. Taylor, G. Gürdal, G. Kumbartzki, N. Benczer-Koller, A. E. Stuchbery, Y. Y. Sharon, M. A. Bentley, Z. Berant, R. J. Casperson, R. F. Casten, A. Heinz, G. Ilie, R. Lüttke, E. A. McCutchan, J. Qian, B. Shoraka, V. Werner, E. Williams, and R. Winkler, *Phys. Rev. C* **83**, 044315 (2011).
- [35] M. Hjorth-Jensen, T. T. S. Kuo, and E. Osnes, *Physics Reports* **261**, 125 (1995).
- [36] A. Blazhev, private communication.